Processing and Application of Ceramics 11 [4] (2017) 265–274
https://doi.org/10.2298/PAC1704265M

A comparative study on the electrical and gas sensing properties of thick films prepared with synthesized nano-sized and commercial micro-sized Fe_2O_3 powders

Ali Mirzaei[1,*], Maryam Bonyani[1], Shahab Torkian[2], Mahdi Feizpour[3], Anna Bonavita[4], Salvatore Gianluca Leonardi[4], Giovani Neri[4]

[1]*Department of Materials Science and Engineering, Shiraz University, Shiraz, Iran*
[2]*Materials Engineering Department, Malek Ashtar University of Technology, Shahin Shahr, Iran*
[3]*Department of Materials Science and Engineering, School of Engineering, Meybod University, P.O. Box 89616-99557, Yazd, Iran*
[4]*Department of Engineering, University of Messina, Contrada di Dio, 98166 Messina, Italy*

Received 6 May 2017; Received in revised form 25 September 2017; Accepted 11 November 2017

Abstract

In this work, Fe_2O_3 nanoparticles (NPs) were successfully synthesized by Pechini sol-gel method. Scanning electron microscopy, transmission electron microscopy and X-ray diffraction characterizations were used to study the morphology and crystal structure of the synthesized products. The electrical and gas sensing behaviour of the synthesized and commercial Fe_2O_3 samples, prepared in the form of thick films, were studied. Though the commercial Fe_2O_3 powders had lower resistance but it was found that the synthesized Fe_2O_3 NPs had better gas sensing properties. The underlying mechanisms are discussed in details. The present findings show advantages of Fe_2O_3 NPs over micro-size particles for gas sensing applications.

Keywords: *Fe_2O_3, Pechini sol-gel, commercial powder, electrical resistance, gas sensor*

I. Introduction

Gases are linked to the life and their odours extremely affect the image of our environment. Even though the human nose serves as a highly advanced sensing instrument which is capable of detecting and distinguishing thousands of different smells with almost instantaneous recognition, it fails if absolute gas concentrations or odourless gases need to be detected. Accordingly, the demand for gas sensing devices which support the human nose is large [1]. Indeed gas detection is obligatory in many different fields, such as industrial monitoring, fuel emission control, automobile exhaust emission control, household security, and environmental pollution monitoring. Therefore, gas sensors are utilized in houses, factories, laboratories, hospitals, and almost all technical installations [2–6].

Ethanol (C_2H_5OH) is one of the most commonly and widely used alcohols in food and chemical industries. Exposure to ethanol vapour results in health problems such as headache, drowsiness, irritation of eyes, liver damage and difficulty in breathing. Furthermore, because of extensive use of ethanol as a beverage, ethanol drinking is one of the main causes of car accidents in the world. Thus the detection of ethanol vapour at ppm levels is of great importance [7,8]. Among the gas sensor devices, conductometric or resistive gas sensors based on metal oxides are the most promising for monitoring ethanol. The success of these types of devices are mainly due to their advantages, such as strong response, high sensitivity, small dimensions, ease of use, portability, rapid response time, simplicity in fabrication, low detection limits, low cost, and low power consumption [9].

Hematite (α-Fe_2O_3), is an n-type metal oxide with band gap of 2.2 eV [7,10]. It has some interesting features, such as low cost, abundance, non-toxicity, ease production and storage, high corrosion resistance, and

*Corresponding authors: tel: +98 71 3721 1984,
e-mail: *alisonmirzaee@yahoo.com*

excellent substrate adhesion [8,11]. Therefore, it is widely utilized in different fields such as catalysts [12], electrode materials [13], batteries [14] solar cells [15] and gas sensors [16,17]. Regarding the gas sensing applications, it is well-known that the size, morphology and shape of sensing materials have a great impact on their chemical and physical properties and consequently in their final gas sensing properties [18,19]. Accordingly, up to date, much efforts have been devoted to the synthesis of different α-Fe_2O_3 nanostructures, such as nanofibers [20] nano spheres [21], nano hollow particles [22] nano rods [23], nanocubes [24], nanotubes [25], nanobelts [26], and nanowires [27], to improve the gas sensing properties of Fe_2O_3. The obtained results suggested that the gas sensitivity of α-Fe_2O_3 can be improved remarkably by optimizing size and shape of α-Fe_2O_3 particles.

As far as the authors know, there is no study concerning the comparison between gas sensing properties of synthesized Fe_2O_3 NPs and commercial Fe_2O_3 powders with larger sizes in the range of a few micro meters. Interestingly, the particle size in the Fe_2O_3 plays an important role in determining the structural characteristics, electronic properties and surface properties (in the form of surface to volume ratio). Regarding gas sensing applications, what is important regarding the particle size is that the electrical resistance of the sensor exposed to air and a target gas undergoes very characteristic changes as particle size changes. Therefore, in this study we synthesized Fe_2O_3 NPs and compared the gas sensing properties with those of commercial Fe_2O_3 powders with larger sizes. We have considered the Fe_2O_3 in the present study due to its low-cost, ease of availability and high stability which are promising features for a gas sensor.

II. Experimental procedure

2.1. Synthesis of Fe_2O_3 NPs

Hydrated iron nitrate ($Fe(NO_3)_3 \times 9\,H_2O$), citric acid ($C_6H_8O_7 \times H_2O$) and poly(ethylene glycol) ($C_2H_6O_2$ - PEG) were purchased from Merck. Double distilled water was used to prepare precursor solutions. Firstly, the appropriate amount of iron nitrate was dissolved in distilled water at 70 °C for 1 h under magnetic stirring to make 0.5 M Fe+3 solution. In a separate flask, citric acid was dissolved in distilled water at 70 °C for 30 min. Afterwards, the citric acid solution was added slowly to the Fe^{3+} solution with a molar ratio (citric acid)/(Fe^{3+} solution) = 2 and it was stirred at 80 °C for 3 h. Then the esterification agent, i.e. PEG, was added with a molar ratio (citric acid)/(PEG) = 2, while stirring and heating the solution. The final solution was refluxed at 150 °C for 2 h. The generated precursor resin was dried at 120 °C for 12 h to obtain the precursor powders. Finally, the amorphous powders were calcined at 550 °C for 3 h in air atmosphere using a muffle furnace to obtain iron oxide NPs. Figure 1 presents the different steps of synthesis procedure. Furthermore, commercial Fe_2O_3 powder was purchased from Sigma-Aldrich with particle sizes of ±5 μm according to specification provided by the company. It is worth noting that we chose the commercial Fe_2O_3 powder only because of its larger particle size relative to our synthesized Fe_2O_3 NPs. In fact, it does not mean that the commercial Fe_2O_3 powders from Sigma-Aldrich are standardly used for sensing purposes.

2.2. Characterization

Phase and crystallinity of the synthesized iron oxide powders were analysed by XRD. Crystallite size was estimated using the Scherrer formula:

$$D = \frac{K \cdot \lambda}{\beta \cdot \cos\theta} \tag{1}$$

where D is the crystallite size, K is the shape factor (0.90), λ is the wavelength of X-rays used (1.5406 Å), β is the full-width at half maximum and θ is the diffraction angle.

Morphological analyses were carried out by scanning electron microscopy (SEM) using ZEISS 1540XB FE SEM instrument coupled with energy dispersive spectroscopy (EDS) and JEOL JEM 2010 transmission electron microscope (TEM-JEOL, Tokyo, Japan) operating at 200 kV.

2.3. Electrical and gas sensing tests

The synthesized and commercial Fe_2O_3 powders were mixed with distilled water and deposited on cleaned Al_2O_3 sensor substrates by drop coating process. Figure 2 shows the sensor substrate and sensor holder. The Al_2O_3 substrate had interdigitated Pt electrodes on the front side and Pt resistive heater on its back. The substrates were prepared commercially.

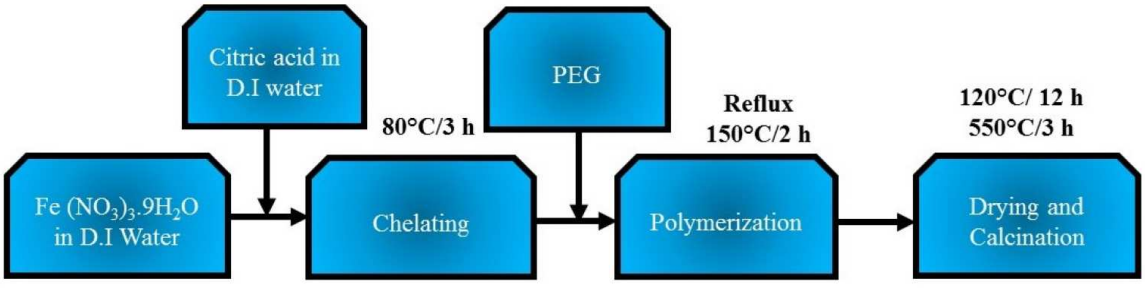

Figure 1. Schematic steps of synthesis procedure

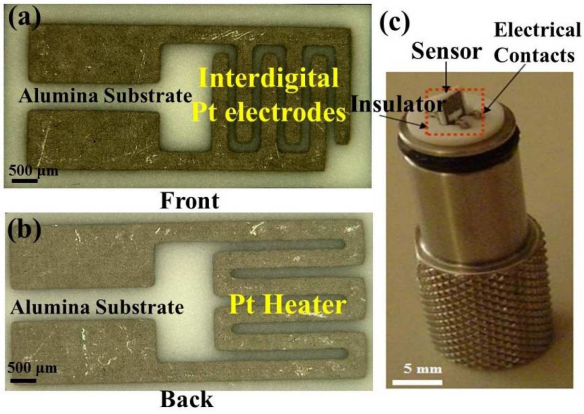

Figure 2. Front side of alumina substrate (a), back side of alumina substrate (b) and sensor holder (c)

Screen printing was used to deposit Pt electrodes on the front side and Pt heater on the back side of alumina substrate. The area of the sensor substrate was 6 × 3 mm. The sensors were tested at different temperatures at various concentrations of ethanol under a synthetic, dry air stream of 100 sccm by collecting the resistance data in the four-point mode.

It should be mentioned that the Pt heater was responsible for temperature control of sensor. Platinum heater was able to reach desired temperature by applying appropriate voltage in a programmed ramp. Relationship between applied voltage (V) to Pt heater and power generated in the heater (P) is as follows:

$$P = \frac{V^2}{R_{heater}} \quad (2)$$

The relationship between P and T for the heater can be shown by fitting equation obtained from increase of temperature measured as a result of applied power:

$$P = 23.35 + 148.725T - 2.17T^2 - 0.559T^3 \quad (3)$$

where units for T and P are [°C] and [W], respectively.

The gas sensing tests were performed by injecting pulses of the target gas from the certified bottles. The change in the resistance of the sensor due to the presence of different gases was measured and the gas response, R, was defined as $R = R_a/R_g$ where R_a is the baseline resistance in air and R_g is the electrical resistance of the sensor in the present of target gas (ethanol). The response and recovery times were defined as the times to reach 90% of the resistance change upon exposure to the target gas and air, respectively.

III. Results and discussion

3.1. Structural characterization of Fe_2O_3 NPs

The phase composition and crystallinity of the synthesized and commercial Fe_2O_3 powders were studied by XRD and shown in Fig. 3a. All reflections in the XRD patterns can be finely indexed to hexagonal phase of Fe_2O_3 (JCPDS Card No. 33-0664). No peaks from other phases were found, suggesting high purity of the synthesized and commercial α-Fe_2O_3 powders. These results are in agreement with literature data [28]. However, the slightly higher crystallinity of commercial Fe_2O_3 powder due to the higher intensity of peaks can be observed. Crystallite size was estimated using the Scherrer formula and (104) plane was chosen for calculation (Fig. 3b). The calculated crystallite sizes are approximately ~23 and ~77 nm for the synthesized and commercial Fe_2O_3 powders, respectively.

Figure 4a shows the low-magnification TEM image

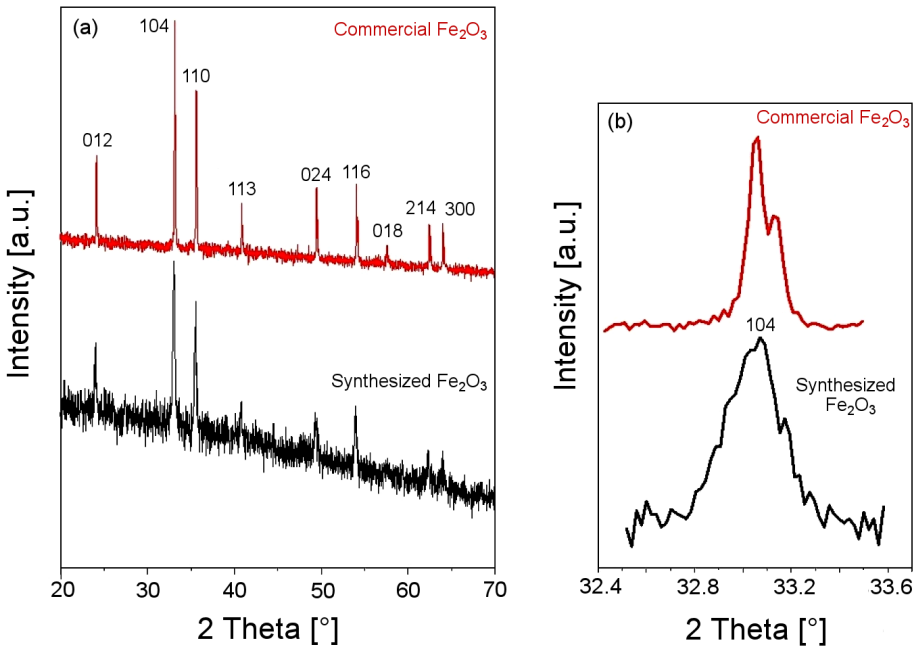

Figure 3. XRD pattern of the synthesized Fe_2O_3 NPs and commercial Fe_2O_3

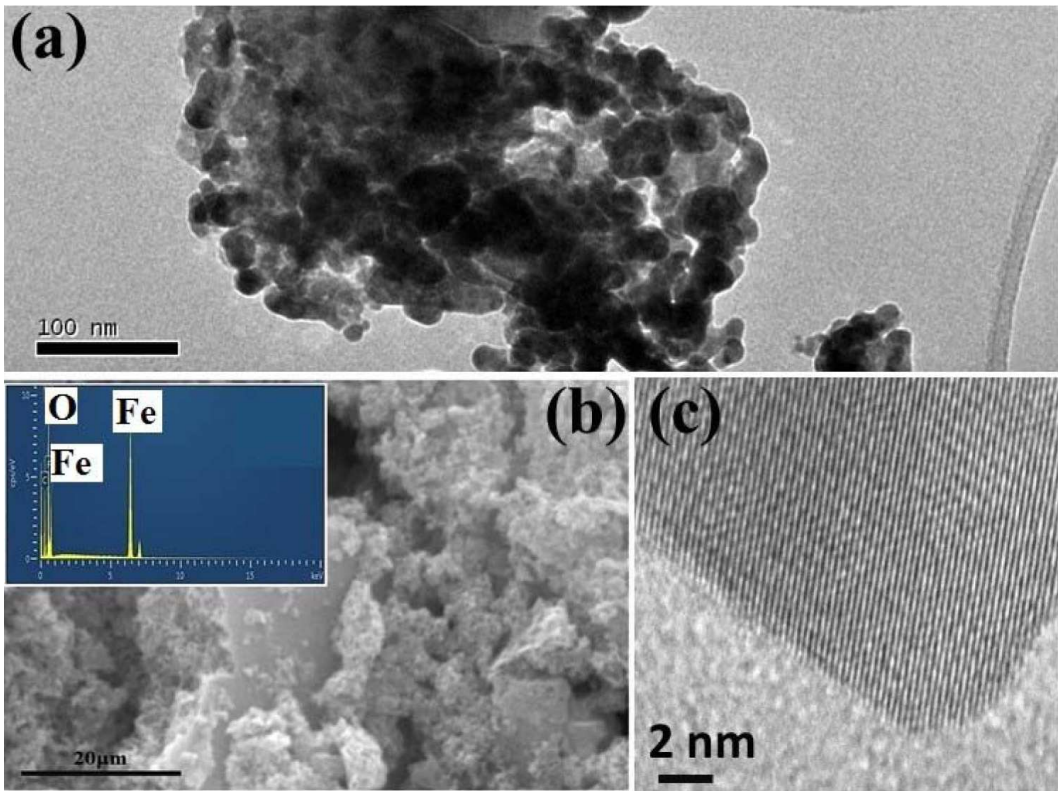

Figure 4. TEM (a), SEM (inset: EDS analysis) (b) and high resolution TEM (c) micrographs of the synthesized Fe_2O_3

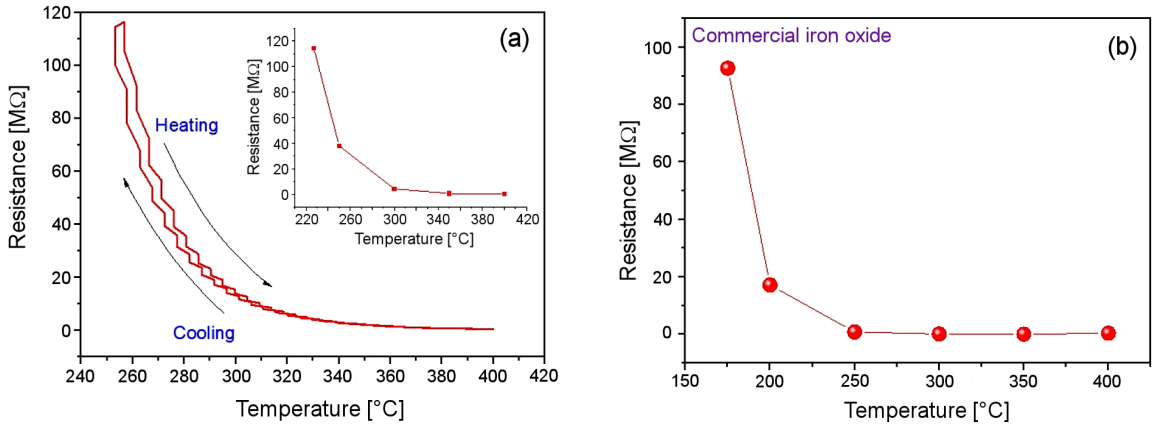

Figure 5. Continuous changes of the electrical resistance of the synthesized Fe_2O_3 upon heating and cooling (resistance vs. *T*) (a) and variations of the resistance of the commercial Fe_2O_3 versus temperature (b)

of the synthesized Fe_2O_3 NPs where the average particle sizes can be estimated to be ~20–50 nm. Figure 4b presents a SEM image of the synthesized Fe_2O_3 on the alumina substrate and the inset of this figure indicates its EDS analysis, showing presence of Fe and O elements, which confirm purity of the synthesized Fe_2O_3 NPs. Good crystallinity of the synthesized Fe_2O_3 NPs is shown in the high-resolution TEM image (Fig. 4c).

3.2. Electrical studies

Since the resistance of the fabricated sensors at room temperature was high and it could not be measured by using the conventional experimental setup, the electrical properties of Fe_2O_3 powders were evaluated in dry air in the range of 175–400 °C for the commercial Fe_2O_3 powders and 225–400 °C for Fe_2O_3 NPs. Figure 5a shows the electrical resistance change of the synthesized Fe_2O_3 NPs sensor during the heating and cooling cycles. As it is clearly seen, the resistance of the sensor on heating and cooling is approximately the same. This means that sensor resistance is very stable upon heating and cooling cycles. Inset of this figure shows variation of the resistance versus the temperature for the synthesized Fe_2O_3 NPs sensor. Also Fig. 5b shows variation of electrical resistance of the commercial Fe_2O_3 powders sensor, where the resistance decreases with the increasing in temperature, demonstrating semiconductor behaviour of Fe_2O_3.

A comparison between the resistances of the sensors shows that the synthesized Fe_2O_3 sensor has a higher

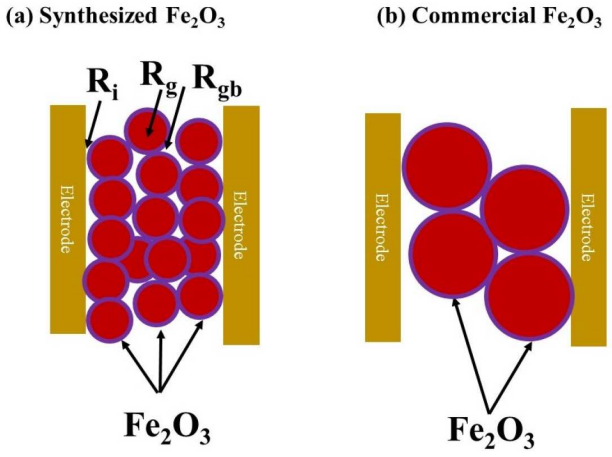

Figure 6. Schematic drawing of the resistances in the synthesized and commercial Fe_2O_3

resistance than the commercial Fe_2O_3 sensor. In fact, with limits of apparatus (120 MΩ), minimum temperature to measure the resistance of the synthesized powder is the range of ~220–225 °C, whereas for the commercial Fe_2O_3 powder it is ~175 °C. In order to explain the high resistance of the synthesized Fe_2O_3 powders, we must consider difference among particle sizes of the sensors as schematically shown in Fig. 6. Between electrodes, there are three kinds of resistances that vary with gas exposure, i.e., the resistance at the oxide-electrode interface (R_i), the resistance at the grain boundary (R_{gb}), and the resistance of grain (R_{grain}). Accordingly, the total sensor resistance (R_{sensor}) is expressed as follows [29]:

$$R_{sensor} = (2R_i - R_{gb}) + N \cdot R_{gb} + N \cdot R_{grain} \qquad (4)$$

where N is the number of particles in the gap between two electrodes. Therefore, it can be seen that the resistance of sensor in air is proportional to the number of particles (N). Thus, for a constant length, fewer particles (larger particles) imply a lower resistance. Since the synthesized Fe_2O_3 NPs have smaller size than the commercial Fe_2O_3, a higher number of particle boundaries are present between the two electrodes for the synthesized Fe_2O_3 NPs than the commercial ones, and therefore, the baseline resistance is higher.

3.3. Gas sensing studies

The operating temperature of the sensor is one of the most important parameters that affect the gas response and response kinetics. The adsorption, desorption, surface coverage, chemical reactions and other related phenomena are temperature activated processes. To find optimum working temperatures for both sensors, they were exposed to 500 ppm ethanol at different temperatures

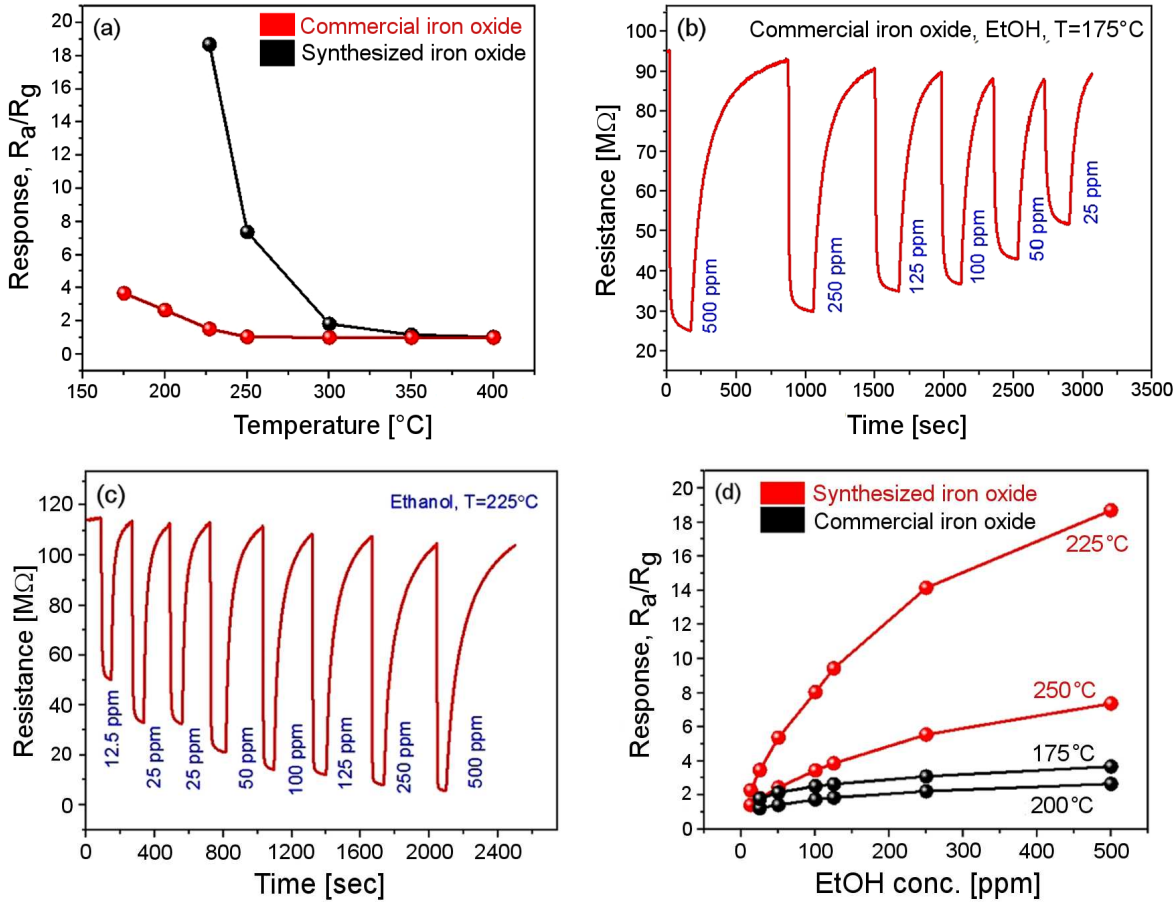

Figure 7. Variations of sensor responses to temperature (a), dynamic responses of the commercial Fe_2O_3 (b) and the synthesized Fe_2O_3 (c) to different values of ethanol and corresponding calibration curves (d)

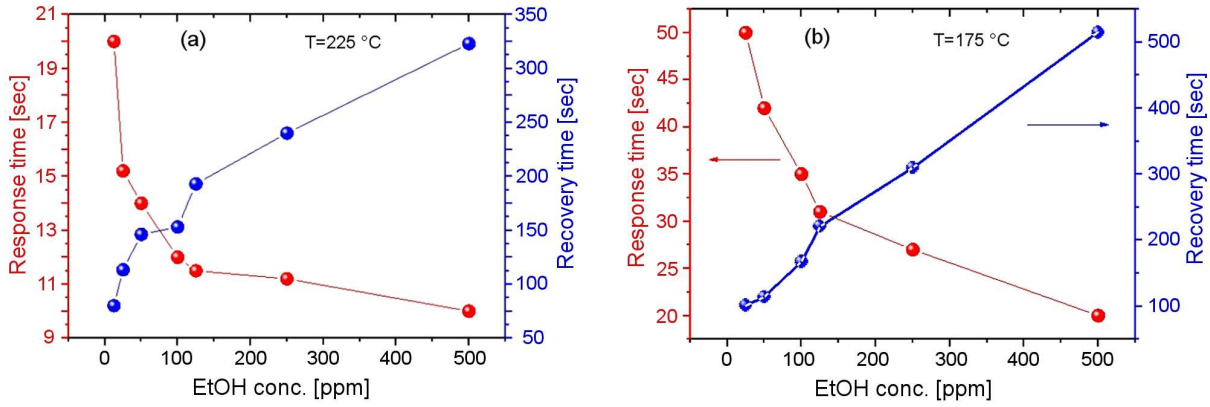

Figure 8. Response and recovery times of: a) synthesized Fe_2O_3 and b) commercial Fe_2O_3

(Fig. 7a). It can be seen that the response of both sensors at low temperatures is higher than at high temperatures. The maximum response of the synthesized Fe_2O_3 NPs sensor occurs at 225 °C, while the optimal working temperature for the commercial Fe_2O_3 sensor is 175 °C. In fact, at higher temperatures the adsorbed ethanol molecules escape before ever reacting with the surface of the sensor or oxygen, resulting in a poor response relative to the optimal temperature [7]. Dynamic responses of the commercial and synthesized Fe_2O_3 sensors to different concentrations of ethanol at their optimal working temperatures are presented in Figs. 7b and 7c, respectively. It can be seen that upon exposure to ethanol, the resistance increases and after stopping ethanol flow the resistance decreases. Therefore, the sensors show n-type behaviour originating from n-type semiconducting behaviour of Fe_2O_3. Furthermore, both sensors show good reversibility because the resistances return to their initial values after injection of synthetic air. Calibration curves of both sensors are shown in Fig. 7d, where it can be clearly seen that the response to all concentrations of ethanol for the synthesized Fe_2O_3 NPs sensor are higher than the response of the commercial Fe_2O_3 sensor. The response of the commercial Fe_2O_3 sensor shows a saturation, where the response is almost constant for high concentrations of ethanol. The response of a sensor depends on the removal of adsorbed oxygen molecules by reaction with the target gas and generation of electrons. Reaction of ethanol with adsorbed oxygen depends on surface coverage by ethanol. According to Langmuir isotherm theory, the fraction of the surface θ covered by adsorption is related to the concentration of the ethanol as follows [30]:

$$\theta = \frac{\alpha \cdot C_{ethanol}}{1 + \alpha \cdot C_{ethanol}} \tag{5}$$

where α is constant and $C_{ethanol}$ is concentration of ethanol. For a small concentration of ethanol exposed to a fixed surface area of the sensor, there is a lower coverage of ethanol molecules on the surface. According to Eq. (5) at sufficiently low concentrations, $\alpha \cdot C_{ethanol}$ is small in comparison with unity, and θ is has a linear proportional to $C_{ethanol}$. An increase in ethanol concentration promotes the surface reaction due to the larger surface coverage. On further increase in the concentration of test gas, the surface reaction shows saturation since a molecule of ethanol which strikes an already occupied site may reflect without adsorption or even displace the occupying molecule. In either case, there is no net effect and surface is totally covered ($\theta \sim 1$) by ethanol gas and there is no increase in sensor's response.

A good sensor must be as fast as possible, so it is very important to study the relationship between response/recovery time and ethanol concentrations. As shown in Fig. 8a, for the synthesized Fe_2O_3 NPs sensor at 225 °C with the increase of ethanol concentration, response time becomes shorter and recovery time becomes longer. For example, the response time for 12.5 ppm ethanol is 21 s and it will decrease to 10 s for 500 ppm ethanol. The same trend is also observed for the commercial Fe_2O_3 sensor (Fig. 8b). The change of the response time can be explained by the varieties of the saturation time and mean residence period of the ethanol molecules on the sensor surface. When ethanol concentration is low, the ethanol molecules may spend a relatively long time reacting with the oxygen ions. With the concentration increasing, the reaction time decreases, and the response time decreases accordingly. The similar regularity is found in the recovery time, which is also attributed to the structure and diffuse velocity. When the air is injected into the test chamber, oxygen molecules will diffuse into the surface to react with the active centres. The complete desorption reaction of inner surface takes more time than the outer surface. It all leads to a long recovery time [7]. Shorter response and recovery times in the synthesized Fe_2O_3 NPs sensor relative to the commercial Fe_2O_3 sensor can be related to the higher working temperature, where the kinetics of adsorption and desorption processes are fast. Furthermore, higher surface area can increase the adsorption reactions.

For an ideal semiconductor gas sensor, the electrical resistance in every gas concentration i.e. at both increasing and decreasing concentration of gas should be the same. However, not all metal oxides semiconductors

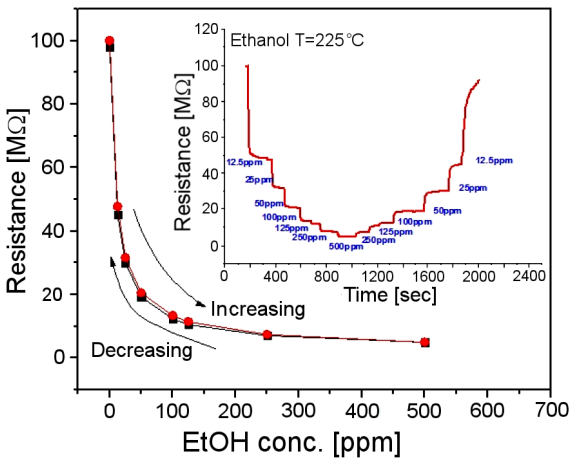

Figure 9. Hysteresis plot of the synthesized Fe_2O_3 upon increasing and decreasing of ethanol concentration

follow the expected ideal trend. To study the hysteresis behaviour of the synthesized Fe_2O_3 NPs sensor, the sensor was exposed to 0 ppm to 500 ppm ethanol over a short period and then the concentration of ethanol was decreased from 500 ppm to 0 ppm. Figure 9 shows the electrical resistance hysteresis plot of Fe_2O_3 NPs sensor as a function of the ethanol concentration at 225 °C. The results show that the sensor has a marginal hysteresis loop area, which demonstrates the good reversibility in the sensor resistance. Hysteresis is mainly associated with porous solids in which the pore size distribution is broad. Hysteresis can be explained by two ways: i) if the solid has pores which are wider in the interior than at the exit and ii) irreversible changes may occur in the structure of the pores on adsorption, and the situation when desorption takes place differs from the situation that existed during adsorption [31]. Therefore, low hysteresis and good reversible nature of the sensor might be due to the intrinsic stability of Fe_2O_3 and narrow pore size distribution of the synthesized Fe_2O_3 NPs.

3.4. Gas sensing mechanism

The gas response of semiconducting metal oxides is measured by the change in their conductivities or resistances upon exposure to oxidizing or reducing gases. The change in conductivity upon exposure to gases can be explained by two different mechanisms: i) a change in the bulk charge carrier concentration due to the formation or annihilation of intrinsic defects such as oxygen vacancies of the gas-sensing materials; and ii) a surface band bending induced by chemisorbed-charged surface species such as oxygen, or the reaction of gas molecules with oxygen adsorbed species [32]. It is widely accepted that the interaction of semiconducting metal oxides and a reducing gas, results in the release of electrons to the conduction band of the semiconductor. This reaction causes an increase in carrier concentration and a macroscopic decrease of the sensor resistance.

When Fe_2O_3 sensors are exposed to air, a certain amount of oxygen from the air adsorbs on their surfaces. The sensor interacts with the adsorbed oxygen by transferring the electrons from their conduction band to the adsorbed oxygen molecules and atoms, resulting in the formation of ionic oxygen species. These processes can be expressed by the following reactions:

$$O_{2(gas)} \longrightarrow O_{2(ads)} \quad (6)$$

$$O_{2(ads)} + e^- \longrightarrow O^-_{2(ads)} \quad (7)$$

$$O^-_{2(ads)} + e^- \longrightarrow 2\,O^-_{(ads)} \quad (8)$$

$$O^-_{(ads)} + e^- \longrightarrow O^{2-}_{(ads)} \quad (9)$$

The adsorbed oxygen species on Fe_2O_3 sensors act as electron acceptors that create a surface depletion layer (Fig. 10a) and band bending (Fig. 10c), which increases the resistance of the sensors. When Fe_2O_3 sensors are exposed to ethanol, these molecules react with the adsorbed oxygen species, thus releasing the captured electrons back to the conduction band, resulting in a decrease of depletion layer thickness and decrease of band bending (Figs. 10b,d). The overall reaction of the ethanol molecules with the ionic oxygen species can be expressed by following reactions:

$$C_2H_5OH_{(ads)} + O^-_{(ads)} \longrightarrow CH_3CHO_{(ads)} + H_2O + e^- \quad (10)$$

$$CH_3CHO_{(ads)} + 5\,O^-_{(ads)} \longrightarrow 2\,CO_2 + H_2O + 5\,e^- \quad (11)$$

$$CH_3CHO_{(ads)} + 6\,O^{2-}_{(ads)} \longrightarrow 2\,CO_2 + 3\,H_2O + 12\,e^- \quad (12)$$

It was observed that the response of the synthesized Fe_2O_3 NPs sensor was higher than the response of the commercial Fe_2O_3 sensor. The advantages of Fe_2O_3 NPs include high specific surface area and more contact potential barriers. The height of the energy barrier for electron transport between neighbouring grains in a material is an important factor for determining the gas sensitivity of that material. From the Arrhenius equation, the conductivity of metal oxides can be described as follows [33]:

$$R = R_0 \cdot \exp\left(-\frac{e \cdot V_s}{k \cdot T}\right) \quad (13)$$

where R_0 is a factor that includes the bulk intragranular resistance, k is the Boltzmann's constant, T is the absolute temperature, and $e \cdot V_s$ is the potential energy barrier at the interface between two neighbouring particles. Also, the mathematical potential energy barrier between two neighbouring grains in semiconducting metal oxide can be described by the following relationship [33]:

$$e \cdot V_s = \frac{e^2 \cdot N_t^2}{2 \cdot \varepsilon_r \cdot \varepsilon_0 \cdot N_d} \quad (14)$$

where N_t is the surface density of adsorbed oxygen ions, $\varepsilon_r \cdot \varepsilon_0$ is permittivity of metal oxide and N_d is the concentration of electron donors. It is clear that both the energy barrier between two grain boundaries and the conductivity of the metal oxides are the functions of the oxygen

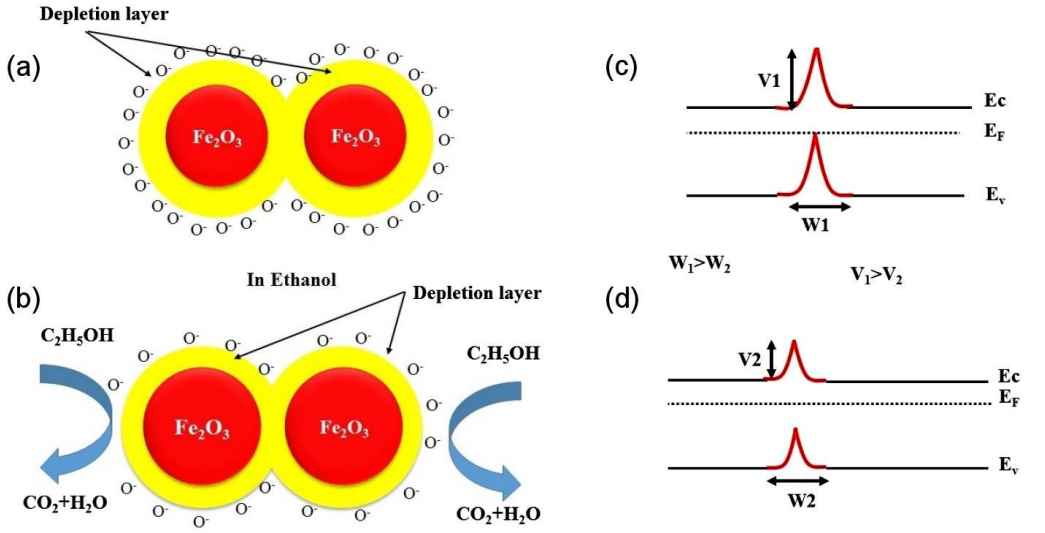

Figure 10. Schematic illustration of sensing mechanism in Fe_2O_3 gas sensor in air (a) and in ethanol (b) and band structure in air (c) and in ethanol (d)

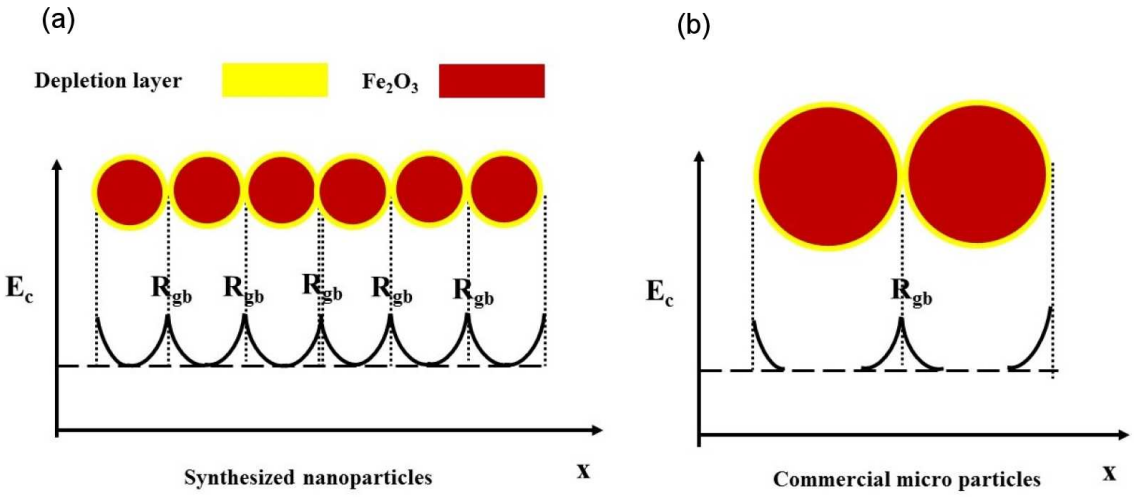

Figure 11. Comparison between potential barriers in the synthesized Fe_2O_3 (a) and commercial Fe_2O_3 (b)

partial pressure, temperature, and doping concentration. The potential energy barrier ($e \cdot V_s$) also depends on the particle size especially when the particle size is in the nanometer scale [34]. Thus, the particle size of the Fe_2O_3 indirectly influences the conductivity and hence the resistance and response of the sensors.

It is well-known that the presence of grain boundaries makes polycrystalline materials more promising for the chemical sensors than single-crystalline or amorphous materials since the grain boundaries play the role of amplifier in resistance during adsorption and desorption processes of gaseous species [35]. In the case of SnO_2 nanofibers, the effects of the size of the particles on sensing properties was studied [36], and it was reported that the samples with smaller nanograins showed superior CO sensing performances than that with larger NPs. It was attributed to the number of potential barriers built at the grain boundaries. In fact nanofibers had smaller grains than that in those with larger grains, which led to a more pronounced modulation of the resistance. The reason for the enhanced response of the synthesized Fe_2O_3 NPs sensor relative to the commercial Fe_2O_3 sensor can be explained using Fig. 11. Ethanol molecules adsorbed on the surface of a Fe_2O_3 NP diffuse into its interior and then they are more likely to cover the grain boundary of the NPs. This produces the electron depleted layers at the surfaces of two adjacent NPs, eventually generating a potential barrier for flow of electrons (Fig. 11a). This potential barrier becomes a resistor, which is connected in series with the potential barriers built around other grain boundaries. As stated before, the change in the resistance during the adsorption of ethanol molecules is the gas sensing mechanism of the sensors. In the sensor fabricated with the commercial Fe_2O_3 powders, the number of potential barriers is fewer (Fig. 11b), resulting in milder change in the re-

sistance at the same gas environment, compared to the sensor fabricated with NPs.

Furthermore, when there are large particles, the surface to volume ratio is decreased. This reduction in the surface to volume ratio reduces effective adsorption of gas which reduces the response or sensitivity of a gas sensor.

Also, it is reported that better crystallinity leads to the enhanced capability to detect target gases. This is because metal oxides with lower crystallinity, which have more structural imperfections, contain a higher number of conducting electrons. This results in a lower degree of resistance modulation in the course of the adsorption and desorption of electrons originating from the interaction of gaseous species on the surface of metal oxides, thus producing an inferior sensor response. However, in the case of the metal oxides with better crystallinity, the number of carriers is lower, which results in a more pronounced modulation of the resistance caused by the adsorption and desorption of the gaseous species [35]. In this study, the effect of reduction of particle sizes down to nano-range was dominant to the effect of crystallinity and consequently the synthesized Fe_2O_3 NPs sensor showed better response.

IV. Conclusions

To summarize, we reported synthesis of Fe_2O_3 NPs by Pechini sol-gel method and compared the electrical resistance and gas sensing properties with those of commercial Fe_2O_3 powders. Different characterization such as SEM/TEM, EDS and XRD were performed. From electrical studies, it was shown that the commercial Fe_2O_3 powders had lower electrical resistance due to the larger particle sizes. Also ethanol gas sensing tests showed that the synthesized Fe_2O_3 NPs sensor had higher optimal working temperature, higher response to ethanol and shorter response and recovery times compare to the commercial Fe_2O_3 sensor. The enhanced gas sensing capabilities were mainly attributed to the higher surface area of the synthesized Fe_2O_3 NPs as a result of the decrease of particle sizes down to nanoscale.

Acknowledgement: Partial support of this study by Iran Nanotechnology Council is greatly acknowledged.

References

1. I. Simon, N. Baarsan, M. Bauera, U. Weimar, "Micromachined metal oxide gas sensors: opportunities to improve sensor performance", *Sensor. Actuat. B*, **73** (2001) 1–26.
2. V.K. Khanna, *Nanosensors Physical, Chemical, and Biological*, First Ed., CRC Press, 2012.
3. A. Mirzaei, K. Janghorban, B. Hashemi, G. Neri, "Metal-core@metal oxide-shell nanomaterials for gas-sensing applications: A review", *J. Nanopart. Res.*, **17** (2015) 1–36.
4. A. Mirzaei, B. Hashemi, K. Janghorban, "α-Fe_2O_3 based nanomaterials as gas sensors", *J. Mater. Sci.: Mater. Electron.*, 27 (2016) 3109–3144.
5. A. Mirzaei, S. Park, G.J. Sun, H. Kheel, C. Lee, S. Lee, "Fe_2O_3/Co_3O_4 composite nanoparticle ethanol sensor", *J. Korean Phys. Soc.*, **69** (2016) 373–380.
6. A. Mirzaei, G. Neri, "Microwave-assisted synthesis of metal oxide nanostructures for gassensing application: A review", *Sensor. Actuat. B*, **237** (2016) 749–775.
7. A. Mirzaei, M. Bonyani, S.G. Leonardi, K.Janghorban, B. Hashemi, G. Neri, "Highly stable and selective ethanol sensor based on α-Fe_2O_3 nanoparticles prepared by Pechini sol-gel method", *Ceram. Int.*, **42** (2016) 6136–6144.
8. S.G. Leonardi, A. Mirzaei, A. Bonavita, S. Santangelo, P. Frontera, F. Panto, P.L. Antonucci, G. Neri, "Comparison of ethanol sensing properties of α-iron oxide nanostructures prepared via sol-gel and electrospinning techniques", *J. Nanotechnol.*, **27** (2016) 075502–075512.
9. A. Mirzaei, S.G. Leonardi, G. Neri, "Detection of hazardous volatile organic compounds (VOCs) by metal oxide nanostructures-based gas sensors: A review", *Ceram. Int.*, **42** (2016) 15119–15141.
10. A. Mirzaei, K. Janghorban, B. Hashemi, A. Bonavita, M. Bonyani, S. G.Leonardi, G. Neri, "Synthesis, characterization and gas sensing properties of Ag@α-Fe_2O_3 core-shell nanocomposites", *Nanomater.*, **5** (2015) 737–749.
11. Z. Li, Z. Lin, N. Wang, Y. Huang, J. Wang, W. Liu, Y. Fu, Z. Wanga, "Facile synthesis of α-Fe_2O_3 micro-ellipsoids by surfactant-free hydrothermal method for sub-ppm level H_2S detection", *Mater. Design*, **110** (2016) 532–539.
12. K. Schou, M.Y. Lin, H.H. Wu, "Studies on the removal of 2-propanol by Ag@Fe_2O_3 core-shell structured catalyst", *J. Taiwan Inst. Chem. Eng.*, **44** (2013) 228–232.
13. M. Nasibi, M.A. Golozar, G. Rashed, "Nano iron oxide (Fe_2O_3)/carbon black electrodes for electrochemical capacitors", *Mater. Lett.*, **85** (2012) 40–43.
14. J. Chen, L.N. Xu, W.Y. Li, "α-Fe_2O_3 nanotubes in gas sensor and lithiumion battery applications", *Adv. Mater.*, **17** (2005) 582–586.
15. S.M. Reda, "Synthesis of ZnO and Fe_2O_3 nanoparticles by sol-gel method and their application in dye-sensitized solar cells", *Mater. Sci. Semiconductor Process.*, **13** (2010) 417–425.
16. J. Zhang, G. Zhu, X. Shen, Z. Ji, K. Chen, "α-Fe_2O_3 nanospindles loaded with ZnO nanocrystals: Synthesis and improved gas sensing performance", *Cryst. Res. Technol.*, **49** (2014) 452–459.
17. A. Mirzaei, S. Park, H. Kheel, G.J. Sun, S. Lee, C. Lee, "ZnO-capped nanorod gas sensors", *Ceram. Int.*, **42** (2016) 6187–619.
18. H. Chen, S.Y. Ma, H.Y. Jiao, G.J. Yang, X.L. Xu, T.T. Wang, X.H. Jiang, Z.Y. Zhang, "The effect microstructure on the gas properties of Ag doped zinc oxide sensors: Spheres and sea-urchin-like nanostructures", *J. Alloys Compd.*, **687** (2016) 342–351.
19. E. Ranjith Kumar, A.S. Kamzin, K. Janani, "Effect of annealing on particle size, microstructure and gas sensing properties of Mn substituted $CoFe_2O_4$ nanoparticles", *J. Magn. Magn. Mater.*, **417** (2016) 122–129.
20. W. Zheng, Z.Y. Li, H.N. Zhang, W. Wang, Y. Wang, C. Wang, "Electrospinning route for α-Fe_2O_3 ceramic nanofibers and their gas sensing properties", *Mater. Res. Bull.*, **6** (2009) 1432–1436.
21. J. Deng, J. Ma, L. Mei, Y. Tang, Y. Chen, T. Lv, Z. Xu, T. Wang, "Porous Fe_2O_3 nanospheres-based H_2S sensor with fast response, high selectivity andenhanced sensitivity", *J. Mater. Chem. A*, **1** (2013) 12400–12403.

22. S. Wang, L. Wang, T. Yang, X. Liu, J. Zhang, B. Zhu, S. Zhang, W. Huang, S. Wu, "Porous a-Fe_2O_3 hollow microspheres and their application for acetone sensor", *J. Solid State Chem.*, **183** (2010) 2869–2876.
23. R. Ramesh, K. Ashok, G.M. Bhalero, S. Ponnusamy, C. Muthamizhchelvan, "Synthesis and properties of α-Fe_2O_3 nanorods", *Cryst. Res. Technol.*, **45** (2010) 965–968.
24. F.H. Zhang, H.Q. Yang, X.L. Xie, L. Li, L.H. Zhang, J. Yu, H. Zhang, B. Liu, "Controlled synthesis and gas sensing properties of hollow sea urchin-like α-Fe_2O_3 nanostructures and α-Fe_2O_3 nanocubes", *Sensor. Actuat. B*, **141** (2009) 381–389.
25. Z. Sun, H. Yuan, Z. Liu, B. Han, X. Zhang, "A highly efficient chemical sensor material for H_2S: α-Fe_2O_3 nanotubes fabricated using carbon nanotube templates", *Adv. Mater.*, **17** (2005) 2993–2997.
26. T.P. Almeida, M.W. Fay, Y.Q. Zhu, P.D. Brown, "In situ TEM investigation of β-FeOOH and α-Fe_2O_3 nanorods", *Phys. E.*, **44** (2012) 1058–1061.
27. L. Liao, Z. Zheng, B. Yan, J.X. Zhang, H. Gong, J.C. Li, C. Liu, Z.X. Shen, T. Yu, "Morphology controllable synthesis of α-Fe_2O_3 1D nanostructures: growth mechanism and nanodevice based on single nanowire", *J. Phys. Chem. C*, **112** (2008) 10784–10788.
28. D. Patil, V. Patil, P. Patil, "Highly sensitive and selective LPG sensor based on α-Fe_2O_3 nanorods", *Sensor. Actuat. B*, **152** (2011) 299–306.
29. J. Tamaki, Y. Nakataya , S. Konishi, "Micro gap effect on dilute H_2S sensing properties of SnO_2 thin film microsensors", *Sensor. Actuat. B*, **130** (2008) 400–404.
30. G.J. Sun, H. Kheel, S. Park, S. Lee, S.E. Park, C. Lee, "Synthesis of TiO_2 nanorods decorated with NiO nanoparticles and their acetone sensing properties", *Ceram. Int.*, **42** (2016) 1063–1069.
31. R. Malherbe, M.A. Ronaldo, *Adsorption and Diffusion in Nanoporous Materials*, Boca Raton, Florida, CRC Press, 2007.
32. M. Batzill, U. Diebold, "Surface studies of gas sensing metal oxides", *Phys. Chem. Chem. Phys.*, **9** (2007) 2307–2318.
33. A.B. Yadava, S. Jit, "Particle size effects on the hydrogen sensing properties of Pd/ZnO Schottky contacts fabricated by sol-gel method", *Int. J. Hydrogen Energy*, **42** [1] (2016) 786–794.
34. G. Zhang, M. Liu, "Effect of particle size and dopant on properties of SnO-based gas sensors", *Sensor. Actuat. B*, **69** (2000) 144–152.
35. A. Katoch, G.J. Sun, S.W. Choi, J.H. Byun, S.S. Kim, "Competitive influence of grain size and crystallinity on gas sensing performances of ZnO nanofibers", *Sensor. Actuat. B*, **185** (2013) 411–416
36. J.Y. Park, K. Asokan, S.W. Choi, S.S. Kim, "Growth kinetics of nanograins in SnO_2 fibers and size dependent sensing properties", *Sensor. Actuat. B*, **152** (2011) 254–260.